Wind Integrated Battery-Super Capacitor Model And Battery Lifetime Analysis

Praseeda Ramesh
Department of EEE
Acharya Institute of Technology
Bangalore , India
praseedaramesh@gmail.com

***Abstract*— A new scheme for improving battery life with the use of super capacitor is presented in this paper. In addition, wind energy is used to charge the battery and super capacitor . The objective of the paper is to deliver a backup power output to the grid during a given time interval. Battery and Super capacitor models have been modelled in Matlab/Simulink and evaluated. Super capacitor s are used to meet the transient load demands during outages. A representative dynamic model of the overall system, incorporating realistic wind-speed and load power variations has been developed. An analysis is presented of the potential improvement in battery lifetime that is achievable by diverting short-term charge/discharge cycles to a super capacitor energy-storage system. This study introduces a method by which super capacitor energy storage systems and control algorithms can be evaluated and implemented in the application area considered. The composition of a prototype test system is described and experimental results are presented to demonstrate system feasibility.**

***Keywords*-Battery, Super capacitor , Wind, DC-DC converter**

Introduction

Secondary lead-acid batteries may have a typical service life of less than 1000 full-cycles [1], [2], and often constitute a large proportion of the total cost of a renewable energy project. The aim of this study is to develop a system to prolong expected battery lifetime, thus reducing battery-replacement costs. This can be a significant advantage, particularly in remote areas, where access can be difficult and costly. In contrast to secondary batteries, super capacitor s also known as "electrochemical double-layer capacitors" (EDLC), or "ultra capacitors," offer higher power density and increased cycle life (of the order of 106 cycles) but have a considerably lower energy density [3]. Super capacitor s currently find use as short-term power buffers or secondary energy storage devices in renewable energy [4], [5], power systems [6], and transport applications [7]–[9].

Combining two or more energy storage systems permits the beneficial attributes from each device to be utilized. The aim of this study is to utilize the inherently high cycle life of super capacitor s in a battery/super capacitor hybrid energy storage system to improve battery lifetime.

Lijun *et al.* [10] have shown that the active hybridization of batteries and super capacitor s can yield an improvement in the overall energy storage system power handling. Wei *et al.* [11] have demonstrated that a battery-super capacitor hybrid has lower battery costs, a general increase in battery life and higher overall system efficiency. Haihua *et al.* [12] have proposed a composite energy storage system with both high power density and energy density for microgrid applications. One similarity between these studies [10]–[12] and others [13]–[16] is that the battery is used to provide the low-frequency component of total power demand whereas the super capacitor provides the short-term or high-frequency component. This has the effect of reducing transient fluctuations in the battery power profile. The work presented here also adopts this approach, and extends previous studies by providing new results which quantify the potential increase in battery cycle lifetime due to the addition of super capacitor energy storage, and describes a means of system implementation and analysis.

I. SYSTEM DESCRIPTION

To demonstrate the proposed system, an example low power (<10 kW) and low battery voltage (<48 Vdc) wind energy conversion system configured, as shown in Fig. 1, was considered. In it, the generated ac voltage from the wind-turbine is rectified and fed to the battery and load via a dc/dc converter operating under maximum power point tracking (MPPT) control such as described by De Broe *et al.* [17]. Relevant application areas include small-scale distributed generation systems [18]–[21] and remote telecom applications [22]–[24]. A dc/ac power converter is used to the convert the battery dc voltage to single-phase ac in this case to supply an ac load.

The proposed system and analysis can also be applied to systems in which the low-voltage battery is interfaced with a regulated dc bus at a higher voltage for power transfer [25]. However, to demonstrate the underlying principle of the system, in this example the battery voltage is used as the effective dc-bus voltage as has been done previously [18]–[21].

II. CURRENT-CONTROLLED DC/DC CONVERTER

Due to turbulent wind power variations and short-term load variations, batteries can be expected to undergo frequent charge/discharge cycling in remote-area wind-power systems.

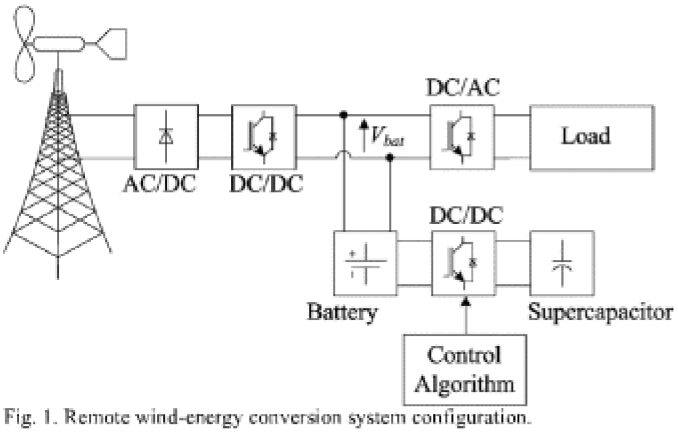

Fig. 1. Remote wind-energy conversion system configuration.

The dc/dc converter under the proposed control strategy filters transient variations from the battery charge-profile in real time by diverting them to/from the super capacitor module. The converter control strategy must therefore be capable of fast, dynamic.

Hysteretic current-mode control can be used to maintain tight regulation of the inductor current in dc/dc converters [26] and gives robust performance despite variation and uncertainty in operating conditions [27]. In addition, this control strategy overcomes the sub harmonic oscillation instability that occurs at duty ratios above 50% with conventional PWM current-mode control [27], [28], which requires the added complexity of slope compensation to resolve [29].

In buck-derived converters, the inductor current is directly proportional to the output current. In contrast, with boost and buck/boost topologies, the inductor current to output current relationship contains an effective duty ratio term making the implementation of boost and buck/boost topologies in this application significantly more complicated. The use of a synchronous buck-converter configured as shown in Fig. 2 is suited to low voltage battery grids (<48Vdc) as the super capacitor voltage can readily be maintained at a higher level than that of the battery. Examples of such systems can be found in small-scale distributed generation [18]–[20] and telecom base-station applications [22], [24].

A. Current-Controlled DC/DC Converter

Assuming ideal components, the governing equation for the inductor current in the converter of Fig. 2 is:

$$L\, dI_L/dt = V_{sc} \cdot u - V_{bat} \qquad (1)$$

The objective of the current controller in this case is to maintain the converter output current by regulating the inductor current to track the command reference current I'. This is done by modulating the power-electronic switch control signal, u, using the following strategy.

A switching function $\sigma = 0$ can be defined as discussed in [30]:

$$\sigma = IL - I' = 0 \qquad (2)$$

where I= command reference current (A).

A switch control strategy for the signal u (see Fig. 2) can be chosen to satisfy (3) such that σ and its time derivative have opposite signs. This ensures that the system will converge to

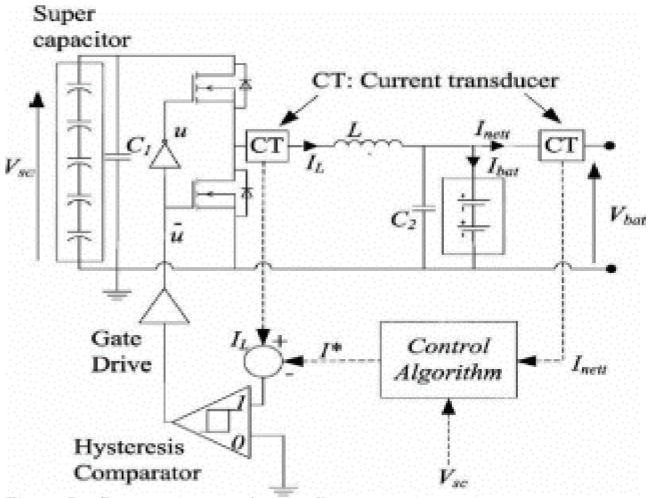

Fig. 2. DC/DC converter and controller.

the state $\sigma = 0$ [31] and consequently the average inductor current converges to the set-point current reference I' [30]:

$$\forall \sigma \_ =/ \ 0 \ : \sigma \cdot d\sigma/dt < 0. \qquad (3)$$

A switching control law, which satisfies condition (3), is defined in (4), where $2h$ is a small constant hysteresis band (100 mA in this case), lying symmetrically about the reference set-point I':

$$u = \begin{cases} u = 1, \text{ if } \sigma < -h \\ u = 0, \text{ if } \sigma > h \end{cases} \qquad (4)$$

For later power conversion efficiency estimation, the approximate switching frequency f_{sw} can be determined from the inductor rise and fall times (T_1 and T_2) in each switch position from (1) as follows [31]:

$$f_{sw} = 1/T_1 + T_2 = 1/(2hL/(V_{sc} - V_{bat})) + (-2hL/-V_{bat}) \qquad (5)$$

B. Control Algorithm

The control algorithm was implemented using an active current-filtering approach to divert the high-frequency component of the system charge/discharge current Inet to the super capacitor , in real time. The controller continuously monitors the incident battery current Inet and sets the converter current reference current I' to cancel the high frequency component of Inet as shown in Fig. 3. Self-discharge causes energy stored in the super capacitor (and consequently the super capacitor voltage) to decay. A super capacitor voltage control loop, with a low, empirically derived static gain, k, was also added as shown in Fig. 3 to maintain the average super capacitor voltage close to a nominal level, $V'sc$ such that $V_{sc} > V_{bat}$.

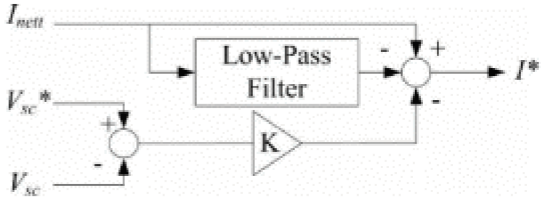

Fig. 3. Control algorithm block diagram.

C. *Experimental Results*

A prototype test system was constructed consisting of four 12 Vdc/75 Ah sealed lead-acid batteries configured with a 24 Vdc nominal voltage. The super capacitor module was made up of twenty two 2.7 Vdc, 1800 F Boostcap super capacitor cells (from manufacturer Maxwell Technologies [32]) connected in series, giving a 60 Vdc nominal voltage. A wind-turbine emulator and programmable-load were used to provide the load and wind-power test profiles (shown in Fig.9). It is beyond the scope of this report to describe the wind turbine and load emulator in detail; however, they were implemented in hardware using power electronic converters with sufficient power control bandwidth to represent the nature of the test profiles used. National Instruments' Labview software was used for test-rig supervisory control and data logging purposes.

The hybrid energy storage system control algorithm was implemented using an industry standard PIC18F4520 microcontroller to calculate the required converter reference current according to the proposed control algorithm (see Fig. 3) in real time. Experimental results showing the recorded net current *I*net and the filtered battery current *I*bat are shown in Fig. 4 with two different low-pass filter time constants. The modified battery current *I*bat can be seen to follow the low-frequency component of the current profile. The battery current contains significantly fewer current polarity reversals than net current *I*net . This indicates that the battery consequently undergoes fewer charge/discharge cycles with the addition of the proposed super capacitor system.

III. SYSTEM SIMULATION

To enable battery-life analysis over longer periods than would be practical by experiment, the proposed system was simulated in the MATLAB / Simulink environment. Conventional simulations employing mean data for renewable resource patterns have been shown to cause short-term fluctuations and associated charge/discharge cycles to be ignored, resulting in underestimation of battery throughput and associated wear [33]. For this reason, a simulation including power variations due to wind turbulence and dynamic load changes was developed with a simulation time step of <1 s.

A. *Battery Model*

The dynamic battery model described in [34] was used to represent battery voltage and state of charge (SOC) variations. A detailed description of the modelling-parameter identification process is given in [35]. For the purpose of this simulation, the battery parameters provided for charge and discharge simulations given in [34] have been used (see the Appendix, Table AI). The number of series battery cells was set to twelve, giving a battery voltage of 24 V at the nominal cell capacity. The governing equations of the lead-acid battery model shown in Fig. 5 from [34] are given later as (6)–(13) with battery-cell model parameters defined in the Appendix, see Table AI:

$$C(I,\theta) = \frac{K_c C_0 (1+\frac{\theta}{\theta_f})^{\varepsilon}}{1+(K_c-1)(I/I^*_{\text{nom}})^k} \qquad (6)$$

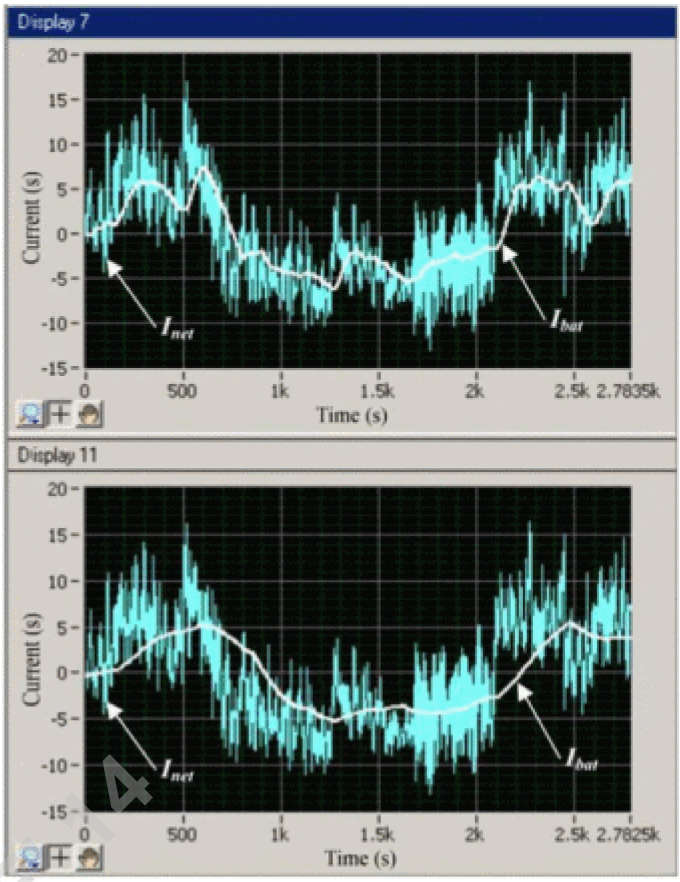

Fig. 4. Measured battery current (white trace) response to a wind and load profile (cyan trace). (a) Low-pass filter time constant = 80 s. (b) Low-pass filter time constant = 300 s.

where K_c, k, and ε are the modeling parameters, I'nom is the battery nominal discharge current, θ is the electrolyte temperature, and θf is the electrolyte freezing temperature (◦C).

State of charge (SOC) and depth of charge (DOC) are defined [34] as:

$$\text{SOC} = 1 - \frac{Q_e}{C(0,\theta)} \text{ where } Q_e = \int_0^t -I_m(t)dt \qquad (7)$$

$$\text{DOC} = 1 - \frac{Q_e}{C(I_{fil},\theta)} \text{ where } I_{fil} = \frac{I_m}{1+\tau_{bs}} \qquad (8)$$

where τ_{bs} is a battery modeling time constant [34]. The equivalent voltage source E_m is given by [34]:

$$E_m(\text{SOC}) = E_{m0} + K_E\,(273 + \theta)\,\ln(\text{SOC}). \qquad (9)$$

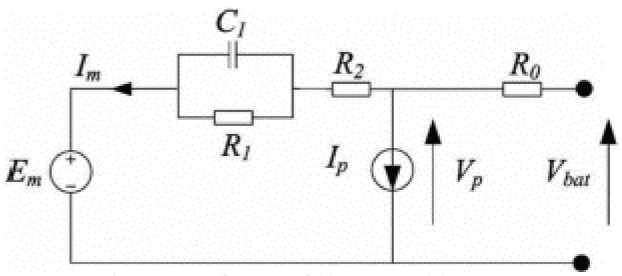

Fig. 5. Dynamic lead-acid battery model [34].

$R0, R1, R2$, and Ip can be determined as follows [34]:

$$R_0\ (\mathrm{SOC}) = R_{00}[1 + A_0(1 - \mathrm{SOC})] \quad (10)$$

$$R_1 = -R_{10} \ln(\mathrm{DOC}) \quad (11)$$

where parameters $R00, A0, R10, R20, A21, A22, Gp0$, and Ap can be found in [34] and in the Appendix; see Table AI.

$$R_2 = R_{20}\frac{\exp[A_{21}(1-\mathrm{SOC})]}{1+\exp(A_{22}I_m/I^*)} \quad (12)$$

$$I_p = V_{pn}G_{p0}\exp\left[\frac{V_{pn}}{V_{po}} + A_p\left(1-\frac{\theta}{\theta_f}\right)\right] \quad (13)$$

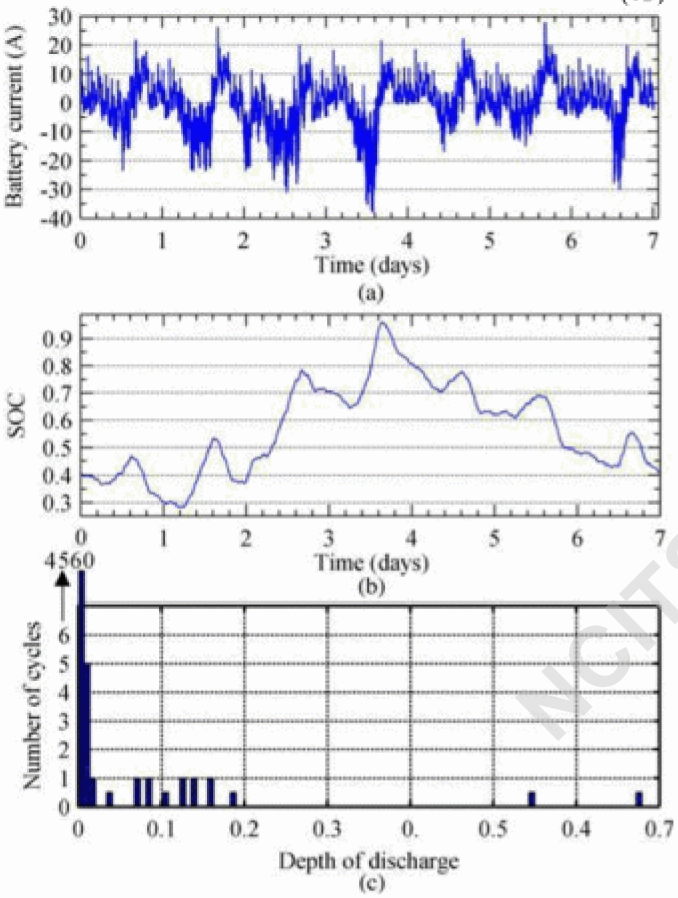

Fig. 6. Battery only system results: (a) battery current, (b) battery state of charge, and (c) histogram of rain-flow cycles (4560 cycles in the range < 0.01).

IV. Results and Discussion

As a base case, the simulation was run with battery energy storage only and with the battery sized such that the load is met at all times. The rain-flow counting algorithm was used to determine the number of cycles experienced by the battery over the week-long simulation period. The battery current, SOC, and the results of the rain-flow cycle counting are shown in Fig. 7 which shows that the battery undergoes 4560 cycles with range <0.01. The simulation was then repeated with the same battery and the super capacitor energy storage system described previously with the low-pass filter time constant set to 3600s. The simulation results are shown in Fig. 8.

In addition the peak current in the hybrid system to be significantly less than in the case of the battery-only system. This decrease in current maxima has an unmodelled benefit in terms of further reducing.

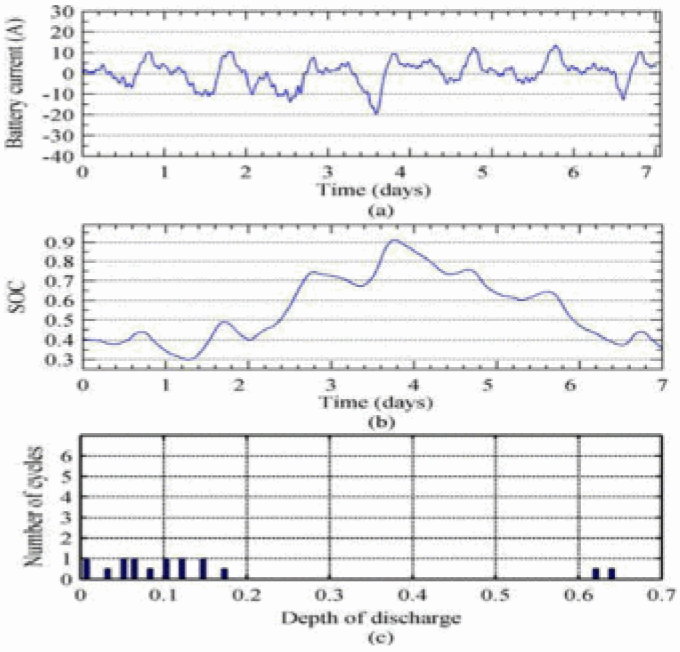

Fig. 7. Hybrid system results: (a) battery current, (b) battery state of charge, and (c) histogram of rainflow cycles.

battery stress as high-current cycling has been shown to increase battery failure rates [51].

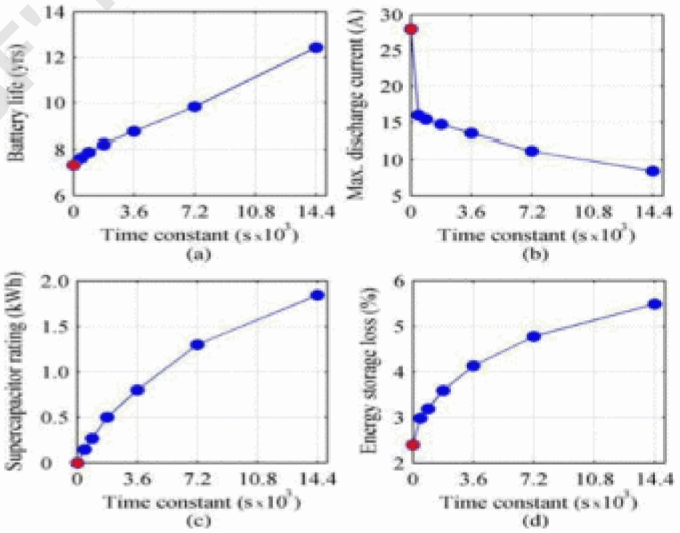

Fig. 8. Simulation results plotted against low-pass filter time constant. Battery-only results shown in red. (a) Battery lifetime estimate. (b) Discharge current maxima. (c) Required super capacitor rating. (d) Energy storage loss as a percentage of energy generated.

VII. Conclusion

This study has investigated the use of super capacitor s to improve expected battery life cycle over a representative weeklong power-profile typical of a small, remote-area wind-energy conversion system. The results show that by diverting transient power variations due to turbulence and short-term load variations to a super capacitor module, battery life cycle can be quantifiably increased. It has also been shown that the battery current maxima can be significantly reduced using the

proposed system. This has an unmodeled benefit in terms of potentially further increasing battery life as high-current cycling has been shown to increase battery failure rates [51].

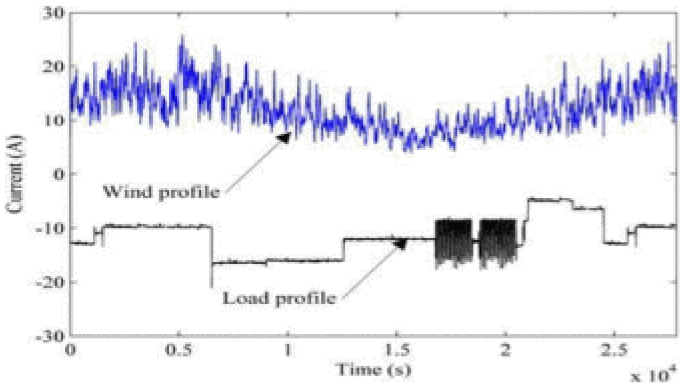

Fig. 9. Synthesized test profiles.

TABLE AI
BATTERY-CELL MODEL PARAMETERS FROM [34]

Parameter	Description	Value
K_c	Empirical constant	1.177
ε	Temperature coefficient	1.29
θ_f	Electrolyte freezing temp.	-40 °C
δ	Empirical constant	1.4
E_{n0}	Full-charge rest voltage	25.62
R_{10}	R1 value at 100% SOC	8.4mΩ
R_{00}	R0 value at 100% SOC	24mΩ
Ke	Empirical constant	70.58 mV/°C
I_{nom}*	Nominal reference current	49A
A_θ	Empirical constant	-0.3
τ_b	RC branch time constant	5000s
C_0	Nominal capacity	261Ah

TABLE AII
DC/DC CONVERTER PARAMETERS (Tj =JUNCTION TEMPERATURE AND Tc = CASE TEMPERATURE)

Parameter	Description	Value
R_l	Power inductor ESR	15mΩ
R_{ds}	MOSFET on resistance	18mΩ (T_j = 25°C)
t_r	MOSFET rise time	220ns (T_c = 25°C)
t_f	MOSFET fall time	200ns (T_c = 25°C)
Q_{rr}	Diode recovery charge	0.6μC (T_j = 25°C)
C_{oss}	MOSFET output capacitance	20nF (T_c = 25°C)

TABLE AIII SUPER CAPACITOR CELL PARAMETERS [38]

Parameter	Description	Value
C_{cell}	Cell nominal capacitance	5000F
R_s	Series resistance (total)	0.33mΩ
R_l	Leakage resistance	351.85Ω
V_{nom}	Rated cell voltage	2.7Vd.c.

TABLE AIV
WIND-TURBINE MODEL PARAMETERS

Parameter	Description	Value
R	Blade radius	1.1m
J_{wt}	Turbine rotor moment of inertia	2.5kg/m^2
J_{elec}	Generator moment of inertia	1kg/ms^2
D'	Damping coefficient	0.00035 Nm/rad/s

REFERENCES

[1] N. Kularatna, "Rechargeable batteries and their management," *IEEE Instrum. Meas. Mag.*, vol. 14, no. 2, pp. 20–33, Apr. 2011.

[2] S. Vazquez, S. M. Lukic, E. Galvan, L. G. Franquelo, and J. M. Carrasco,"Energy storage systems for transport and grid applications," *IEEE Trans.Ind. Electron.*, vol. 57, no. 12, pp. 3881–3895, Dec. 2010.

[3] L. Peiwen, "Energy storage is the core of renewable technologies," *Nanotechnol. Mag.*, vol. 2, no. 4, pp. 13–18, Dec. 2008.

[4] Q. Liyan and Q. Wei, "Constant power control of DFIG wind turbines with super capacitor energy storage," *IEEE Trans. Ind. Appl.*, vol. 47, no. 1, pp. 359–367, Jan. 2011.

[5] M. Uzunoglu and M. S. Alam, "Dynamic modeling, design, and simulation of a combinedPEM fuel cell and ultracapacitor system for stand-alone residential applications," *IEEE Trans. Energy Convers.*, vol. 21, no. 3, pp. 767–775, Sep. 2006.

[6] B. P. Roberts and C. Sandberg, "The role of energy storage in development of smart grids," *Proc. IEEE*, vol. 99, no. 6, pp. 1139–1144, Jun. 2011.

[7] A. Khaligh and L. Zhihao, "Battery, ultracapacitor, fuel cell, and hybrid energy storage systems for electric, hybrid electric, fuel cell, and pluginhybrid electric vehicles: State-of-the-art," *IEEE Trans. Veh. Technol.*,vol. 59, no. 6, pp. 2806–2814, Jul. 2010.

[8] P. Thounthong, V. Chunkag, P. Sethakul, B. Davat, and M. Hinaje, "Comparative study of fuel-cell vehicle hybridization with battery or super capacitor storage device," *IEEE Trans. Veh. Technol.*, vol. 58, no. 8,pp. 3892–3904, Oct. 2009.

[9] P. Thounthong and S. Rael, "The benefits of hybridization," *IEEE Ind.Electron. Mag*, vol. 3, no. 3, pp. 25–37, Sep. 2009.

[10] G. Lijun, R. A. Dougal, and L. Shengyi, "Power enhancement of an actively controlled battery/ultracapacitor hybrid," *IEEE Trans. Power Electron.*, vol. 20, no. 1, pp. 236–243, Jan. 2005.

[11] L. Wei, G. Joos, and J. Belanger, "Real-time simulation of a wind turbinegenerator coupled with a battery super capacitor energy storage system," *IEEE Trans. Ind. Electron.*, vol. 57, no. 4, pp. 1137–1145, Apr. 2010.

[12] Z. Haihua, T. Bhattacharya, T. Duong, T. S. T. Siew, and A. M. Khambadkone, "Composite energy storage system involving battery and ultracapacitor with dynamic energy management in microgrid applications," *IEEE Trans. Power Electron.*, vol. 26, no. 3, pp. 923–930, Mar. 2011.

[13] F. Liu, J. Liu, and L. Zhou, "A novel control strategy for hybrid energy storage system to relieve battery stress," in *Proc. 2010 IEEE Int. Symp. Power Electron. Distrib. Gener. Syst.*, Hefei, China, Jun. 2010, pp. 929– 934.

[14] A. M. van Voorden, L. M. R. Elizondo, G. C. Paap, J. Verboomen, and L. van der Sluis, "The application of super capacitors to relieve batterystorage systems in autonomous renewable energy systems," in *Proc. IEEE Power Tech. 2007*, Lausanne, Switzerland, Jul. 2007, pp. 479–484.

[15] L. Wei and G. Joos, "A power electronic interface for a battery super capacitor hybrid energy storage system for wind applications," in *Proc. IEEE Power Electron. Spec. Conf. 2008*, Rhodes, Greece, 2008, pp. 1762–1768.

[16] J. Yan, R. Shibata, N. Yamamura, and M. Ishida, "A control method of

prolonging the service life of battery in stand-alone renewable energy system using electric double layer capacitor (EDLC)," in *Proc. Int. Conf. Power Electron. Drives Syst. 2005*, Kuala Lumpur, Malaysia, 2005, pp. 228–233.

[17] A. M. De Broe, S. Drouilhet, and V. Gevorgian, "A peak power tracker for small wind turbines in battery charging applications," *IEEE Trans. Energy Convers.*, vol. 14, no. 4, pp. 1630–1635, Dec. 1999.

[18] L. Kuo-Yuan, C. Yaow-Ming, and C. Yung-Ruei, "MPPT battery charger for stand-alone wind power system," *IEEE Trans. Power Electron.*, vol. 26, no. 6, pp. 1631–1638, Jun. 2011.

[19] Z. M. Salameh and A. B. Cultura, "Small scale distributed generation system at University of Massachusetts Lowell," in *Proc. IEEE Power Energy Soc. General Meeting*, Minneapolis, MN, 2010, pp. 1–6.

[20] F. Giraud and Z. M. Salameh, "Steady-state performance of a gridconnected rooftop hybrid wind-photovoltaic power system with battery storage," *IEEE Trans. Energy Convers.*, vol. 16, no. 1, pp. 1–7, Mar. 2001.

[21] F. Valenciaga and P. F. Puleston, "Supervisor control for a stand-alone hybrid generation system using wind and photovoltaic energy," *IEEE Trans. Energy Convers.*, vol. 20, no. 2, pp. 398–405, Jun. 2005.

[22] G. Fabbri, A. J. M. Cardoso, C. Boccaletti, and A. Girimonte, "Control and optimisation of power consumption in Radio Base stations," in *Proc. IEEE 33rd Int. Telecommun. Energy Conf.*, Amsterdam, The Netherlands, 2011, pp. 1–6.

[23] G. Rami, T. Tran-Quoc, N. Hadjsaid, and J. L. Mertz, "Energy supply for remote base transceiver stations of telecommunication," in *Proc. IEEE Power Eng. Soc. General Meeting, 2004*, Denver, CO, 2004, pp. 1916– 1921.

[24] G. Schmitt, "The green base station," in *Proc. 4th Int. Conf. Telecommun.—Energy Special Conf.*, Vienna, Austria, 2009, pp. 1–6.

[25] C. Yuan-Chih and L. Chang-Ming, "Establishment of a switched reluctance generator-based common DC microgrid system," *IEEE Trans. Power Electron.*, vol. 26, no. 9, pp. 2512–2527, Sep. 2011.

[26] T. Szepesi, "Stabilizing the frequency of hysteretic current-mode DC/DC converters," *IEEE Trans. Power Electron.*, vol. 2, no. 4, pp. 302–312, Oct.1987.

[27] M. Castilla, J. M. Guerrero, J. Matas, J. Miret, and J. Sosa, "Comparative study of hysteretic controllers for single-phase voltage regulators," *IET Power Electron.*, vol. 1, no. 1, pp. 132–143, Mar. 2008.

[28] O. Trescases, A. Prodic, and N. Wai Tung, "Digitally controlled currentmode DC-DC converter IC," *IEEE Trans. Circuits Syst.*, vol. 58, no. 1, pp. 219–231, Jan. 2011.

[29] R. B. Ridley, "A new, continuous-time model for current-mode control [power convertors]," *IEEE Trans. Power Electron.*, vol. 6, no. 2, pp. 271– 280, Apr. 1991.

[30] R. Venkataramanan, A. Sabanovic, and S. Cuk, "Sliding mode control of DC-to-DC converters," in *Proc. IEEE Int. Conf. Ind. Electron. Control Instrum.*, San Francisco, CA, Nov. 1985, pp. 251–258.

[31] V. Utkin, *Sliding Modes in Control and Optimization*. Berlin: Springer- Verlag, 1992.

[32] Maxwell Technologies, Inc., San Diego, CA. (Sep. 2011). [Online]. Available: www.maxwell.com

[33] A. J. Ruddell, A. G. Dutton, H.Wenzl, C. Ropeter, D. U. Sauer, J.Merten, C. Orfanogiannis, J. W. Twidell, and P. Vezin, "Analysis of battery current microcycles in autonomous renewable energy systems," *J. Power Sources*, vol. 112, pp. 531–546, Aug. 2002.

[34] M. Ceraolo, "New dynamical models of lead-acid batteries," *IEEE Trans.Power Syst.*, vol. 15, no. 4, pp. 1184–1190, Nov. 2000.

[35] S. Barsali and M. Ceraolo, "Dynamical models of lead-acid batteries: implementation issues," *IEEE Trans. Energy Convers.*, vol. 17, no. 1, pp. 16–23, Mar. 2002.

[36] C. Yonghua, "Assessments of energy capacity and energy losses of super capacitor s in fast charging-discharging cycles," *IEEE Trans. Energy Convers.*, vol. 25, no. 1, pp. 253–261, Mar. 2010.

[37] P. Thounthong, S. Rael, and B. Davat, "Analysis of super capacitor as second source based on fuel cell power generation," *IEEE Trans. Energy Convers.*, vol. 24, no. 1, pp. 247–255, Mar. 2009.

[38] Ultracapacitor Products datasheet. 2008. Nesscap Co. Ltd, Gyeonggi-do, Korea. [Online]. Available: http://www.nesscap.com/ product/edlc_large1.jsp

[39] J. Klein. AN-6005 Synchronous buck MOSFET loss calculations with Excel model. Fairchild Semiconductor Corporation, San Jose, CA. (Apr. 2006). [Online]. Available: http://www.fairchildsemi.com/an/AN/AN- 6005.pdf

[40] PolarTM Power MOSFET IXFN140N20P datasheet. Ixys Corporation.
Milpitas, CA. (May 2008). [Online]. Available: http://ixapps.ixys.com/ DataSheet/99245.pdf

[41] PolarTM Power MOSFET IXFN140N30P datasheet. Ixys Corporation.
Milpitas, CA. (May 2008). [Online]. Available: http://ixapps.ixys.com/
DataSheet/DS99571F(IXFN140N30P).pdf

[42] A. D. Diop, E. Ceanga, J. R´etiveau, J. M´ethot, and A. Ilinca, "Real-time
three-dimensional wind simulation for windmill rig tests," *Renew. Energ.* vol. 32, pp. 2268–2290, Oct. 2007.

[43] C. Nichita, D. Luca, B. Dakyo, and E. Ceanga, "Large band simulation
of the wind speed for real time wind turbine simulators," *IEEE Trans. Energy Convers.*, vol. 17, no. 4, pp. 523–529, Dec. 2002.

[44] I. Munteanu, A. I. Bratcu, N. A. Cutululis, and E. Ceanga, *Optimal Control of Wind Energy Systems—Towards a Global Approach*. London: Springer-Verlag, 2008.

[45] S. Heier, *Grid Integration of Wind Energy Conversion Systems*. Chichester, U.K.: John Wiley, 1998.

[46] H. Bindner, T. Cronin, P. Lundsager, J. F. Manwell, U. Abdulwahid, and
I. Baring-Gould, "Lifetime modelling of lead acid batteries," Risø Nat. Lab., Roskilde, Denmark, Apr. 2005.

[47] [47] J. F. Manwell, A. Rogers, G. Hayman, C. Avelar, and J. G. McGowan, "Hybrid2 Theory Manual," Dept. Mech. Eng., Univ. Massachusetts, Amherst, MA, 1998.

[48] "Deep-Cycle Gel Battery Datasheet. Trojan Battery Company. Santa Fe Springs, CA. (Apr. 2008). [Online]. Available: http://www.trojanbattery.
com/pdf/GEL_SS_Web.pdf

[49] S. D. Downing and D. F. Socie, "Simple rainflow counting algorithms," *Int. J. Fatigue*, vol. 4, pp. 31–40, 1982.